applied sciences

MDPI

Article

Intelligent Timber Damage Monitoring Using PZT-Enabled Active Sensing and Intrinsic Multiscale Entropy Analysis

Shuai Guo [1,2], Tong Shen [1,2], Li Li [1,2], Huangxing Hu [1,2], Jicheng Zhang [3] and Zhiwen Lu [1,2,*]

[1] Key Laboratory of Metallurgical Equipment and Control Technology, Ministry of Education, Wuhan University of Science and Technology, Wuhan 430081, China
[2] Hubei Key Laboratory of Mechanical Transmission and Manufacturing Engineering, Wuhan University of Science and Technology, Wuhan 430081, China
[3] School of Urban Construction, Yangtze University, Jingzhou 434023, China
* Correspondence: luzhiwen@wust.edu.cn

Abstract: Timber has been commonly used in the field of civil engineering, and the health condition of timber is of great significance for the whole structure in practical scenarios. However, due to mechanical load and environmental impact, timber-based constructions are vulnerable to termite attack, microbial corrosion and fractures within their service lives. Thus, the damage monitoring of timber structures is very challenging under real situations. This paper presents an intelligent timber damage monitoring approach using Lead Zirconate Titanate (PZT)-enabled active sensing and intrinsic multiscale entropy analysis. The proposed approach adopts PZT-enabled active sensing to collect the signals depicting dynamic characteristics of the timber structure. The proposed intrinsic multiscale entropy analysis utilizes variational mode decomposition (VMD) to deal with the collected response signals. Decomposition of the response signals into a set of band-limited intrinsic mode functions (BLIMFs) denoting nonlinear and nonstationary characteristics. Then multiscale sample entropy (MSE) is employed to extract quantitative features, which are adopted as health condition indicators of timber structures. Finally, the convolutional neural network (CNN) fulfills the intelligent timber damage monitoring by using the quantitative features as the effective input. The research findings reveal the efficacy and superiority of the proposed method.

Keywords: timber damage monitoring; active sensing; variational mode decomposition; multiscale sample entropy; convolutional neural network

Citation: Guo, S.; Shen, T.; Li, L.; Hu, H.; Zhang, J.; Lu, Z. Intelligent Timber Damage Monitoring Using PZT-Enabled Active Sensing and Intrinsic Multiscale Entropy Analysis. *Appl. Sci.* **2022**, *12*, 9370. https://doi.org/10.3390/app12189370

Academic Editor: Raffaele Zinno

Received: 26 August 2022
Accepted: 15 September 2022
Published: 19 September 2022

1. Introduction

Timber is a common material utilized in timber-framed buildings, furniture products, composite materials, timber-based panels and other products [1]. However, timber itself has disadvantages of easy corrosion, rain erosion and insect damage. Due to the degradation of its physical properties, natural environmental and other damage, timber-framed buildings suffer different types of damage, such as cracking, decay, insect damage, tenon pulling and bending deformation [2,3]. This timber damage leads to performance degradation and subsequently destruction of the overall structure [4]. If the damage is not detected in time, it can cause serious catastrophes in some significant structures. Thus, accurate timber damage monitoring is very important in reducing the upkeep costs and ensuring the safety of the whole structure [5].

In the field of health monitoring of machinery and building structures, a piezoelectric material called Lead Zirconate Titanate (PZT) is usually utilized because it is equipped with the merits of strong piezoelectric effect, affordability, fast response, dual ability of actuation, sensing and energy harvesting capacity [6,7]. Wide-ranging frequency vibrations are produced and detected by PZT transducers. As a result, PZT can efficiently produce and detect ultrasonic waves to achieve timber damage monitoring.

The vital part of timber damage monitoring is feature extraction of ultrasonic waves. The collected timber damage ultrasonic signals are typically nonlinear and nonstationary [8,9]. The extraction of damage characteristics from ultrasonic signals is of vital importance in timber damage monitoring. The common signal processing algorithms include Fourier transform [10], wavelet transform (WT) [11], empirical mode decomposition (EMD) [12,13], Hilbert Huang transform (HHT) [14] and variational mode decomposition (VMD) [15]. Fourier transform extracts the frequency information of the signal, but has insufficient ability in processing nonlinear and nonstationary signals [16]. WT better depicts the frequency characteristics of signal, but there exists the shortfall that the wavelet basis function needs to be selected manually [17]. EMD is a fully adaptive time-frequency analysis algorithm. Nonlinear and nonstationary signals can be broken down into approximately stationary modes with different frequency scales, namely intrinsic mode functions (IMFs) [18]. EMD and Hilbert transform are combined to form HHT. As a core of HHT, EMD has advantages of full adaptivity and is capable of handling nonlinear and nonstationary signals, while it also has disadvantages such as mode aliasing problem. In 2014, Dragomiretskiy et al. [19] put forward an optimized adaptive algorithm called VMD. It uses a variational way to decompose a nonlinear and nonstationary signal into band-limited intrinsic mode functions (BLIMFs) non-recursively. Compared to EMD, VMD has stronger noise robustness, faster calculation speed and stronger anti-interference ability. Thus, it has been widely used in feature extraction of nonlinear and nonstationary signals [20].

With the continuous development of nonlinear theories, entropy-based quantitative features have been adopted in mechanical fault diagnosis and structural health monitoring [21,22]. The common entropy theories include approximate entropy (AE) [23], sample entropy (SE) [24], permutation entropy [25], etc. SE is an improved AE algorithm, and avoids tedious self-matching, template matching and eliminates inconsistent statistical quantities in AE [26]. Thus, SE is suitable for measuring the complicacy and regularity of short time series and has been extensively utilized in the field of structural health monitoring. Bandt et al. [27] proposed permutation entropy based on the idea of comparing adjacent values to determine the complicacy of time series. The typical single scale analysis used in traditional entropy theories ignores the feature information present on numerous scales. Later, Costa et al. [28] put forward a multiscale derivation algorithm for traditional SE, namely multiscale sample entropy (MSE). MSE accurately and comprehensively captures the dynamical characteristics of time series from the view of numerous scales. MSE has been widely used in the fields of signal processing and mechanical fault diagnosis [29]. Previous research has confirmed the efficiency and superiority of MSE [30,31]. It should be noted that the quantitative features extracted by entropy-based theories can be used as the input of neural networks to realize intelligent fault diagnosis and structural health monitoring. Intelligent health monitoring has become a research hotspot due to machine learning technology's rapid development [32,33]. Convolutional neural network (CNN) [34] is a kind of classical algorithm in deep learning, which has been extensively used in the fault diagnostic domains and structural health monitoring domains, due to its advantages of extracting feature information adaptively and pattern recognition [35]. CNN-integrated approaches can effectively process massive and high-dimensional datasets, while avoiding noise interference and low accuracy in condition identification.

This paper presents a novel intelligent timber damage monitoring approach using PZT-enabled active sensing and intrinsic multiscale entropy analysis. The PZT-generated response signals are divided into multiple sets of BLIMFs using VMD. MSE values of certain orders of BLIMFs are calculated and adopted as quantitative features denoting timber health conditions. Thus, the intrinsic multiscale entropy analysis obtains the quantitative features of multiple BLIMFs at multiple scales, which provides the feature matrices for subsequent CNN-integrated machine learning. Section 2 reviews the methodologies involved with intrinsic multiscale entropy analysis, which consists of VMD, MSE and the typical structure of CNN. Section 3 illustrates the proposed intelligent timber damage monitoring approach by giving its detailed steps. Section 4 introduces the whole apparatus

setup and experimental procedures. Section 5 verifies the proposed intelligent timber damage monitoring approach by experimental data processing and comparative experiment. Section 6 concludes the paper by presenting the major findings and essential discussion.

2. Methodologies

2.1. Variational Mode Decomposition

VMD is a brand-new adaptive time-frequency analysis algorithm based on the ideas of Wiener filtering, Hilbert transform and heterodyne demodulation [36]. This algorithm fulfills the adaptive decomposition of the signal in a completely non-recursive way. It has a strict mathematical theoretical foundation, good anti-noise effect and fast calculation speed [37]. VMD decomposes the signal $x(t)$ into k orders of BLIMFs $u_k(t)$. The center frequency of kth order BLIMF is ω_k. In EMD, the signal's component, whose mean value of the upper and lower envelopes determined by the local maximum and local minimum points equals zero, is defined as IMF, while VMD redefines BLIMF as an AM-FM signal to establish the variational model. The expression of BLIMF is as follows:

$$u_k(t) = A_k(t)\cos(\varphi_k(t)) \tag{1}$$

where $\varphi_k'(t) = \omega(t) = d\varphi_k(t)/dt$ is the instantaneous frequency and $A_k(t)$ is the amplitude. During period $[t-\delta, t+\delta]$, where $\delta = 2\pi/\varphi_k'(t)$, $u_k(t)$ is regarded as a harmonic signal. The steps of establishing the variational model are as follows:

(1) Hilbert transform is performed on each BLIMF $u_k(t)$. To obtain the unilateral spectrum of $u_k(t)$, an analytical signal is constructed, i.e., $(\delta(t) + j/\pi t) * u_k(t)$, where $\delta(t)$ represents Dirichlet function and $*$ is the convolutional symbol.
(2) The analytical signal of each BLIMF is mixed with a pre-estimated center frequency. Each BLIMF's spectrum is transferred to the fundamental frequency range, i.e., $[(\delta(t) + j/\pi t) * u_k(t)]e^{-j\omega_k t}$.
(3) By demodulating the L_2 norm of the signal gradient, the bandwidth of each BLIMF is estimated.
(4) By introducing constraints, the following optimal variational model is constructed:

$$\begin{aligned} &\min_{\{u_k\},\{\omega_k\}} \left\{ \sum_k \| \partial_t \left[\left(\delta(t) + \tfrac{j}{\pi t}\right) u_k(t) \right] e^{-j\omega_k t} \|_2^2 \right\} \\ &\text{s.t.} \sum_k u_k = f \end{aligned} \tag{2}$$

where $u_k = \{u_1, u_2, \ldots, u_k\}$ are BLIMFs, and $\omega_k = \{\omega_1, \omega_2, \ldots, \omega_k\}$ are center frequencies corresponding to each BLIMF.

The quadratic penalty factor α and Lagrange multiplication operator λ are utilized to build the extended Lagrange function $L(\{u_k\}, \{\omega_k\}, \lambda)$ to arrive at the best solution for the variational model discussed above:

$$\begin{aligned} L(\{u_k\}, \{\omega_k\}, \lambda) = \alpha \sum_k \left\| \partial_t \left[\left(\delta(t) + \tfrac{j}{\pi t}\right) u_k(t) \right] e^{-j\omega_k t} \right\|_2^2 \\ + \left\| f(t) - \sum_k u_k(t) \right\|_2^2 + \left\langle \lambda(t), f(t) - \sum_k u_k(t) \right\rangle \end{aligned} \tag{3}$$

Thus, the limited variational problem becomes an unconstrained problem. Among this unconstrained problem, the quadratic penalty factor ensures accuracy of signal reconstruction and the Lagrange multiplier ensures the strictness of model constraints. The main steps of the VMD algorithm are as follows:

(1) Input signal $x(t)$;
(2) Initialize $\hat{u}_k^1, \omega_k^1, \hat{\lambda}^1$ and n;

(3) Update u_k and ω_k;

$$\hat{u}_k^{n+1}(\omega) = \frac{\hat{f}(\omega) - \sum_{i \neq k} \hat{u}_i(\omega) + \frac{\hat{\lambda}(\omega)}{2}}{1 + 2\alpha(\omega - \omega_k)^2} \tag{4}$$

$$\omega_k^{n+1} = \frac{\int_0^\infty \omega |\hat{u}_k(\omega)|^2 d\omega}{\int_0^\infty |\hat{u}_k(\omega)|^2 d\omega} \tag{5}$$

(4) Update λ;

$$\hat{\lambda}^{n+1}(\omega) = \hat{\lambda}^n(\omega) + \tau \left[\hat{f}(\omega) - \sum_{k=1}^{k} \hat{u}_k^{n+1}(\omega) \right] \tag{6}$$

(5) The convergence is judged according to the following equation. If the convergence condition is met, the decomposition process ends. Otherwise, return to steps (2) and (3) to continue decomposition until the stopping condition is met.

$$\frac{\sum_k \left\| \hat{u}_k^{n+1} - \hat{u}_k^n \right\|_2^2}{\left\| \hat{u}_k^n \right\|_2^2} < e \tag{7}$$

2.2. Multiscale Sample Entropy

MSE sheds light on the complicacy and nonlinearity of fluctuations across various time scales, which was put forward to conduct the measurement of the SE on numerous scales. It has extraordinary stability and interference-fighting capability [30,31], assuming that the time series contain points $x_1, x_2, x_3, \ldots x_N$ sampled every millisecond, for the reason that the initial time scale τ is 1 ms. In order to create various scales and resolutions of the signal, coarse graining the data fundamentally refers to conducting the averaging on consecutive points. The following are the specific computation steps for the MSE:

(1) At scale one, the coarse-grained time series are the initial time series.
(2) At scale two, the coarse-grained time series can be created by averaging two successive time points as presented in Figure 1a. Defining that $y_1 = (x_1 + x_2)/2$; $y_2 = (x_3 + x_4)/2$ and so on.

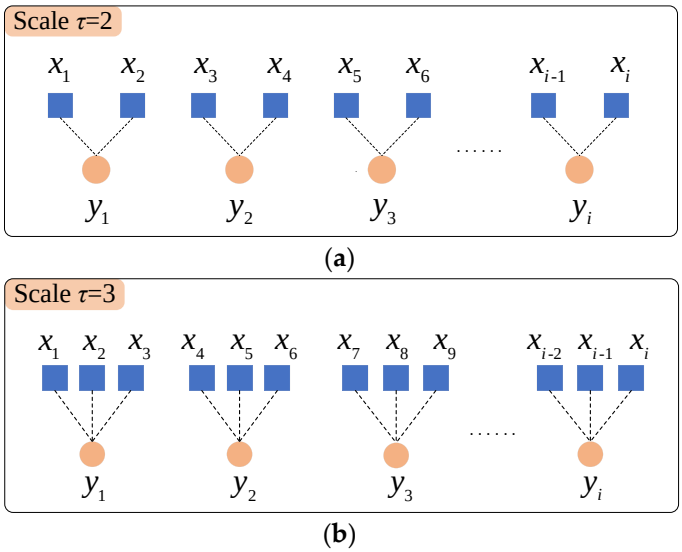

Figure 1. The illustration of conventional coarse-graining procedure: (**a**) τ is 2; (**b**) τ is 3.

(3) At scale three, as illustrated above, the average of three consecutive time points forms the coarse-grained time series shown in the Figure 1b. That is, define $y_1 = (x_1 + x_2 + x_3)/3$; $y_2 = (x_4 + x_5 + x_6)/3$ and so on.

Mathematically, the above procedures can be transformed into a number of coarse-grained time series $\{y_j^{(\tau)}\}$:

$$y_j^{\tau} = \frac{1}{\tau} \sum_{i=(j-1)\tau+1}^{j\tau} x_i, j = 1, 2, \ldots, N/\tau \tag{8}$$

where τ is the time scale. The coarse-grained series $y_j^{(\tau)}$, where $j = 1, 2, \ldots, N$ are the original series when the time scale τ =1. When $\tau > 1$, the coarse-grained time series has a length of N/τ. The detailed procedures of MSE are displayed in Figure 2.

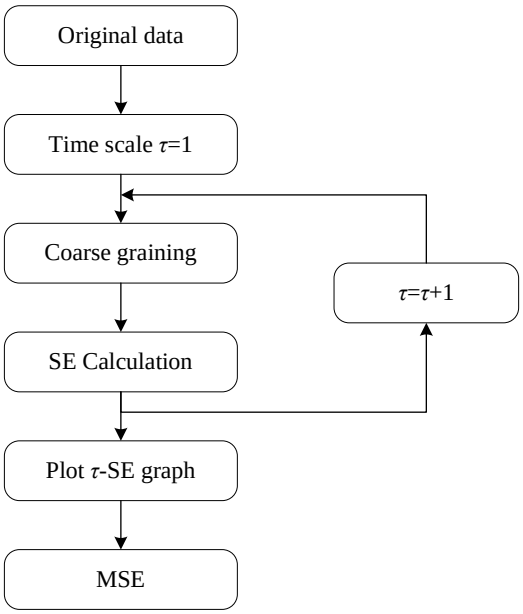

Figure 2. The illustration of MSE procedures.

The SE of each time series $y_j^{(\tau)}$ is calculated under the embedded dimension; to choose scale factors to quantify signal nonlinearity, the connection between SE and time scale factor is plotted. The SE value reveals the correlation of the signal under this scale factor. The relationship between SE and MSE is shown below:

$$E_{MSE}(x, \tau, m, r) = E_{SE}(y^{\tau}, m, r) = -\mathrm{In}(n_r^{m+1}/n_r^m) \tag{9}$$

where m is the embedding dimension. r is tolerance. $E_{SE}(\cdot)$ is sample entropy. The coarse-grained sequence's n_s^m and n_s^{m+1} space vectors have dimensions of m and $(m + 1)$, respectively. It should be noted that a larger time scale τ contributes to more accurate presentation of a signal's regularity and complexity based on theoretical derivation of MSE, while it results in more computational load. Taking both the presentation of the signal's regularity and the algorithm's efficiency into consideration, and after several experimental trials, the scale factor is chosen as 20 in our application research.

2.3. Convolutional Neural Network

CNN has achieved considerable success in the image processing industry and is one of the most representative deep learning network designs [38]. The advantages of CNN over other classification algorithms are that CNN has a strong generalization ability and

learns the best features to represent the objects in the photos. Convolutional, Pooling, ReLU and Fully Connected layer make up CNN's four layers [39].

(1) A convolutional layer is made up of several filters that are applied to the input data in layers. The width, height and weights of each filter are used to extract features from the input data. The weights in the filter start out with random values during the training phase and are learnt in the training set. In the convolutional layer, each filter stands in for a feature and finds a match. Therefore, a huge number is generated by the convolutional operation, activating the filter to that feature. CNN uses this procedure to find out the best filters to describe the object [40].
(2) The ReLU (Rectified Linear Unit) layer is an activation layer connected after a convolutional layer and causes the network to become non-linear [41]. The ReLU aids the network in learning more difficult decision-making functions and lessens overfitting.
(3) The pooling layer is used to minimize the dimensionality of the feature maps while retaining the crucial information [42]. In the pooling layer, a filter applies the pooling operation to the input data by sliding over it in the pooling layer.
(4) Input, hidden and output layers make up the MultiLayer Perception (MLP) that constitutes the fully connected layer [43]. The features produced by the CNN are sent to the input layer. A MLP is made up of one or more hidden layers, each hidden layer a series of neurons with weights that will be learned during the training step. There are also a series of neurons in the output layer.

The convolutional and the dense steps make up the bulk of the typical structure of a CNN model. The former learns which features are most useful to extract from the images and the latter learns how to categorize the features. The structure of the CNN model is displayed in Figure 3.

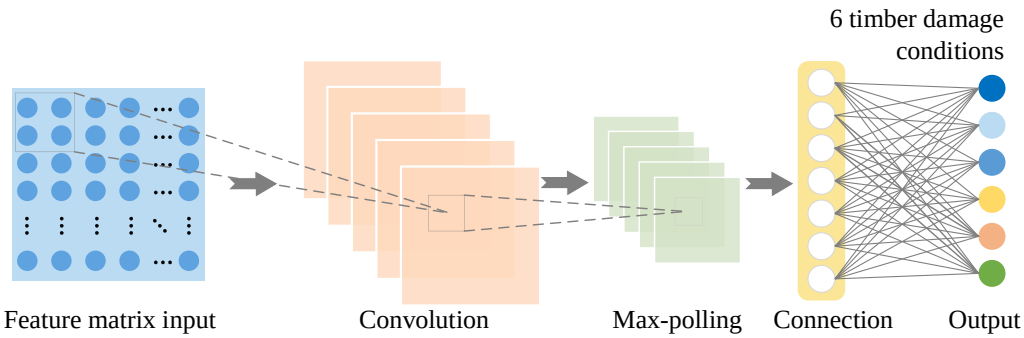

Figure 3. The structure of the CNN model.

3. The Proposed Intelligent Timber Damage Monitoring Approach Using PZT-Enabled Active Sensing and Intrinsic Multiscale Entropy Analysis

Aiming at diagnosing timber damage, a novel approach based on multiscale entropy analysis and CNN is proposed in this paper. VMD decomposes PZT generated response signals into multiple sets of BLIMFs. Then MSE values of certain orders of BLIMFs are calculated and adopted as quantitative features denoting timber health conditions. The main steps of the proposed approach are presented as follows:

(1) VMD is used to process the PZT generated response signals and the multiple sets of BLIMFs containing a large number of nonlinear and nonstationary damage characteristics are obtained.
(2) Then, MSE values of specific orders of BLIMFs are calculated and used as indicators of the state of the timber health.
(3) Two-dimensional feature matrices are constructed and randomly divided into training set, validation set and test set. The data of the training set and validation set are input into CNN for training and the parameters are adjusted during the training process to obtain a neural network model with good recognition.

(4) The trained CNN model is utilized to justify the data of the test set to realize the monitoring of timber damage.

4. Experimental Setup and Procedures

4.1. Timber Specimens

In the experimental test, the timber is pine wood from North America, which has a density of 420 kg/m^2 and moisture content of around 19.2%. The experimental samples' dimensions are 0.04 m broad, 0.15 m long and 0.08 m deep. As shown in Figure 4, epoxy was used to install two PZT patches at the predefined positions on a total of six specimens. As a result, the interface between PZT and the surface of the timber was covered with a thin layer of epoxy resin. A PZT material layer is sandwiched between two electrode layers in a PZT sensor [44]. The diameter of the PZT sensor was 10 mm and the thickness was 0.2 mm. The total of six specimens were divided into three groups. As manifested in the Figure 4, some artificial structural damage was applied to all specimens before monitoring. A crack existed on each specimen for Group A (specimens 1 and 2). A hole was drilled in each specimen for Group B (specimens 3 and 4) and C (specimens 5 and 6). The PZT patches' locations and pre-configured damage are shown in Figure 4.

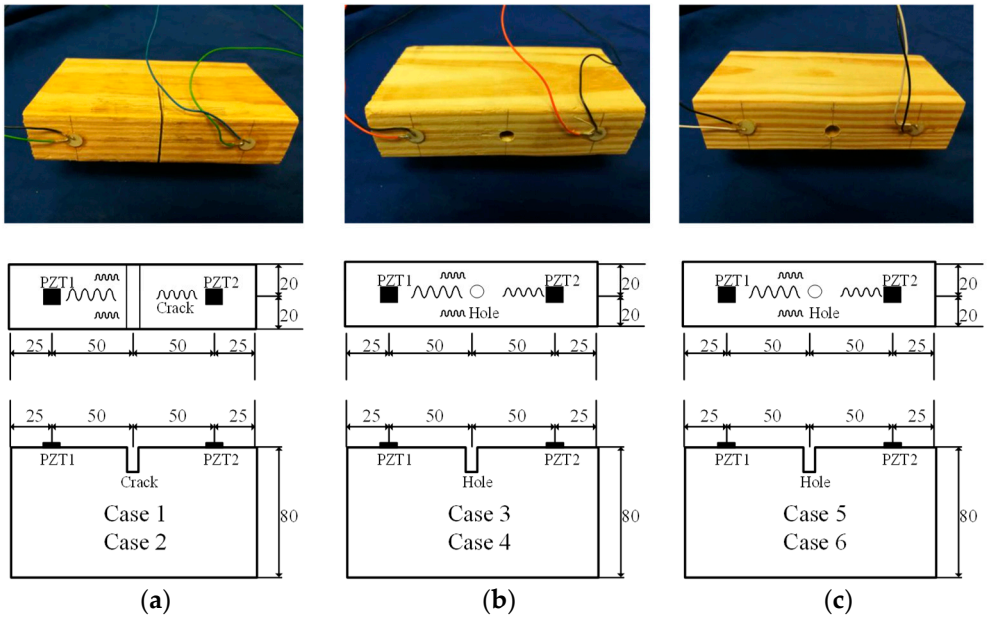

Figure 4. Timber specimens of three groups. (**a**) Specimen of Group A; (**b**) Specimen of Group B; (**c**) Specimen of Group C.

Groups A, B, and C were subjected to three types of artificial damage, different crack depths, different depths and diameters of the holes under different circumstances, in this experimental test. For Group A, the crack width of both specimens was fixed at 1.5 mm while the artificial crack damage depths varying from 4 to 10 mm were conducted; in Group B, for both specimens, the holes' diameter was set at 4 mm while the effect was researched by varying the artificial hole depths in 4 and 10 mm under two circumstances; As for the last Group C, to look into the impact of this structural flaw, the depth of the hole for the two test specimens was set at 4 mm and the hole diameters were varied between 3 and 9 mm. Table 1 illustrates the test cases of specimens in this research.

Table 1. Test circumstances of specimens for three groups.

Group A	Case 1	Case 2	Group B	Case 3	Case 4	Group C	Case 5	Case 6
Crack width	1.5	1.5	Hole diameter	4	4	Hole diameter	3	9
Crack depth	4	10	Hole depth	4	10	Hole depth	4	4

4.2. Experimental Setup and Experimental Procedures

The experimental setup is depicted in Figure 5a, which also includes a control computer, a fixed piece of timber and a data gathering system (NI USB-6361). The data gathering system samples at a rate of 2 MS/s. In each instance, a sine wave signal was used to stimulate the PZT actuator, which then produced guided stress waves coming from one side of the timber specimen. The response signal was captured by the PZT sensor on the opposite side. The excitation signal had the following characteristics: a starting frequency of 100 Hz, a stopping frequency of 300 kHz, an amplitude of 10 V and a period of 1 s. In this investigation, a frequency step size of 50,000 was used. All tests were finished in the lab in under two hours to reduce the effects of environmental humidity on the outcomes. The humidity and temperature during the conducted experiment are around 64% and 26 °C, respectively. The schematic diagram of the apparatus is displayed in Figure 5b.

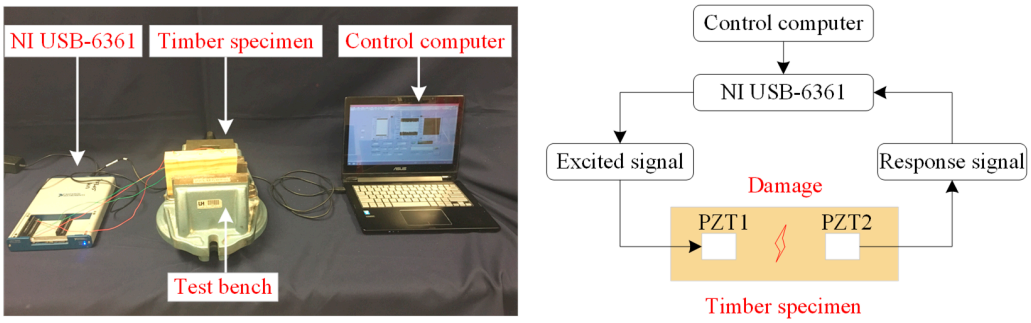

(**a**) (**b**)

Figure 5. (**a**) A photo of the apparatus, (**b**) The schematic diagram of the apparatus.

5. Application Research for Timber Damage Monitoring

The PZT sensors' time domain signal responses for Case 1-Case 6 are shown in Figure 6, respectively. Each curve represents a cycle, or 1 s in the time domain, of the sensor signal response to the sine wave signal. Different groups of piezoelectric ceramic sensors receive signals differently as a result of the various damage modes.

In our research, 540 sets of sine wave signals of crack damage and hole damage in the experiment were selected for research. After the signal processing was performed in the above manner, the obtained two-dimensional feature matrices were all 7×7 size, which were used to characterize each type of timber damage. According to the width and depth of cracks and the diameter and depth of holes, 540 groups of sine wave signals were divided into six different wear conditions. For each working condition, the training set, validation set, and test set were all randomly chosen at a ratio of 3:1:1 and the data of the training set and validation set were fed into the CNN for training. Simultaneously, the hyper parameters were optimized and adjusted in the training process to obtain a neural network model with good recognition effect and complete the discrimination of six different timber damage states. Theoretically, the more convolutional layers of the network, the more extracted features can reflect the characteristics of the original data. For classification problems with multiple categories and large samples, CNN often uses multiple convolutional layers. However, for classification problems with few categories and samples, with there are more and more network layers, redundant network layers may be generated and the model may be unstable and overfitted [45]. Therefore, considering the parameters of the model and the training effect, it is sufficient to use one or two convolutional layers for 540 samples of six timber damage conditions. Through multiple experimental comparisons, the structural parameters of the model are given in Table 2.

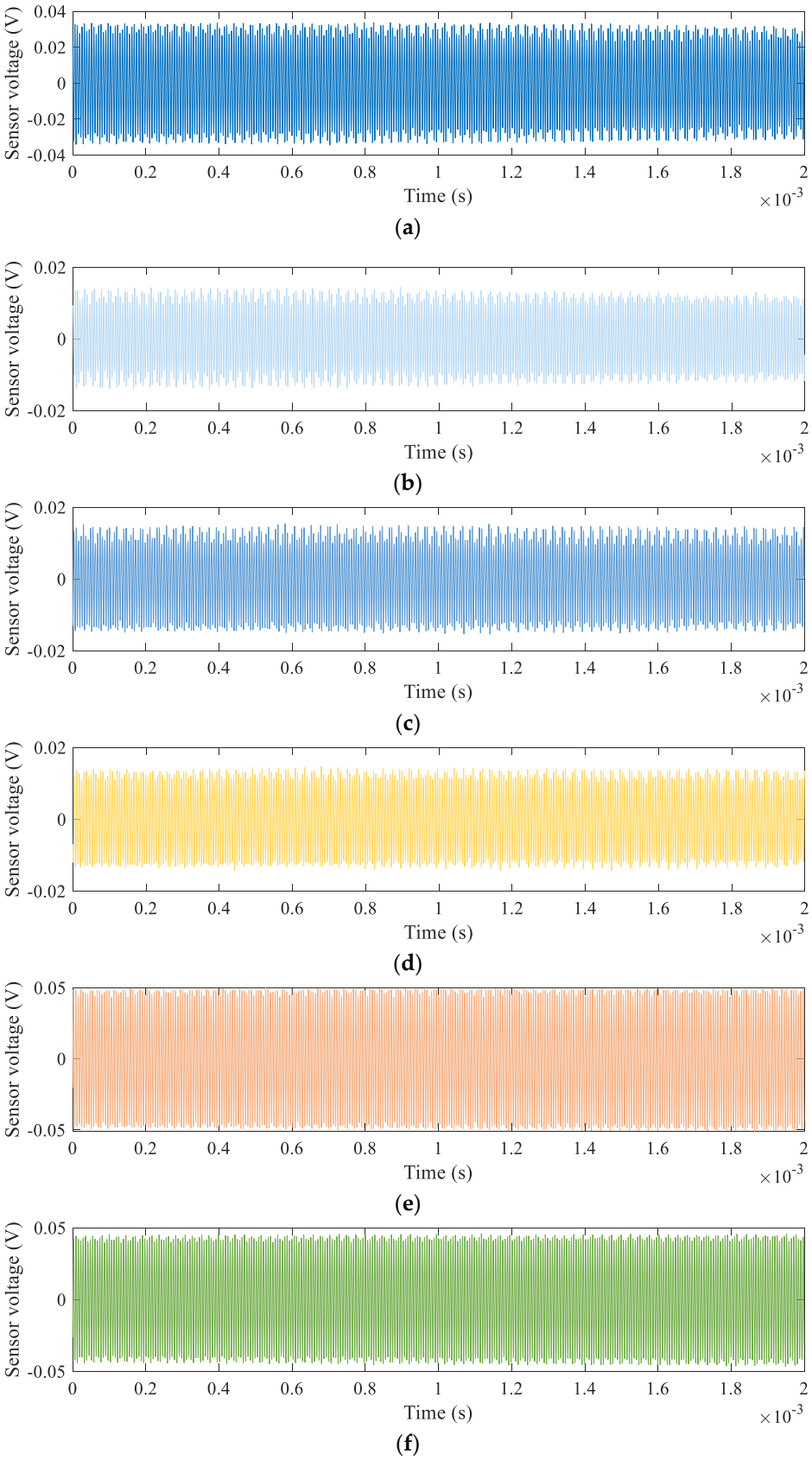

Figure 6. Sensor signal response of each type of timber damage mode. (**a**) Case 1, (**b**) Case 2, (**c**) Case 3, (**d**) Case 4, (**e**) Case 5, (**f**) Case 6.

The hyper parameter setting of CNN can directly affect the efficiency and accuracy of the model. Through many experiments, the final main setting of the CNN model in this paper was: two convolutional layers, of which the filter size was set as 3×3, the step size was 1, the number of convolution cores was 64 and the size of the pooling layer was 2×2. The pooling mode was the maximum pooling layer, the activation function was the Rectified Linear Unit (ReLU), the optimizer was SGD, the learning rate was 0.0001 and batch processing had a value of 4. CNN's framework is based on Tensorflow's Keras. The Tensorboard visualization tool was used to view the variations of accuracy curve, loss function curve and other curves. A total number of 2000 iterative trainings were conducted in the experiment. The variation curves of accuracy and loss function in the training process are displayed in Figure 7.

Table 2. CNN model structure.

Network Layers (Type)	Out SHAPE
Input Layer	(None, 7, 7, 1)
Conv2d	(None, 7, 7, 32)
Batch_Normalization	(None, 7, 7, 32)
Max_Pooling2d	(None, 3, 3, 32)
Conv2d_1	(None, 3, 3, 64)
Batch_Normalization_1	(None, 3, 3, 64)
Flatten	(None, 64)
Dense	(None, 1024)
Dropout	(None, 1024)
Dense_1	(None, 6)

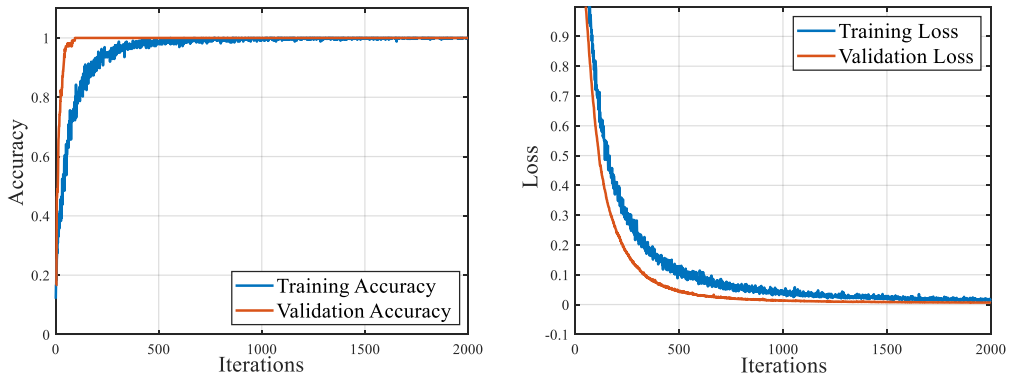

(**a**) (**b**)

Figure 7. (**a**) The accuracy of training set and validation set; (**b**) The loss function of training set and validation set.

Figure 7 demonstrates how the accuracy of the training set and validation set gradually increases as the number of iterations rises and, after 400 iterations, the accuracy of both the training set and the validation set reaches 100%, without obvious shock. The loss function lowers monotonically with the increasing number of iterations and stabilizes in a low range. After 2000 iterations, the final training loss and test loss are close to 0 and there is no fitting phenomenon, which indicates that the method has good diagnostic effect. In order to intuitively display the classification outcomes, we used the confusion matrix to represent the discrimination outcomes, as displayed in Figure 8.

To demonstrate the superiority of the approach in this paper, it was compared with ALIF, EMD and EEMD decomposition algorithms and the same dataset was utilized for the test. To avoid the randomness of the test results, the above method was used for 10 repetitive experiments. The average accuracy of different methods for timber damage classification is demonstrated in Table 3.

It can be seen from Table 3 that the classification accuracy of the approach proposed in this paper achieves the highest results. The classification results of timber damage conditions are the best when compared to the results obtained by other algorithms. The experimental results validate the efficacy and superiority of the proposed approach for detecting timber damage based on VMD, MSE and CNN.

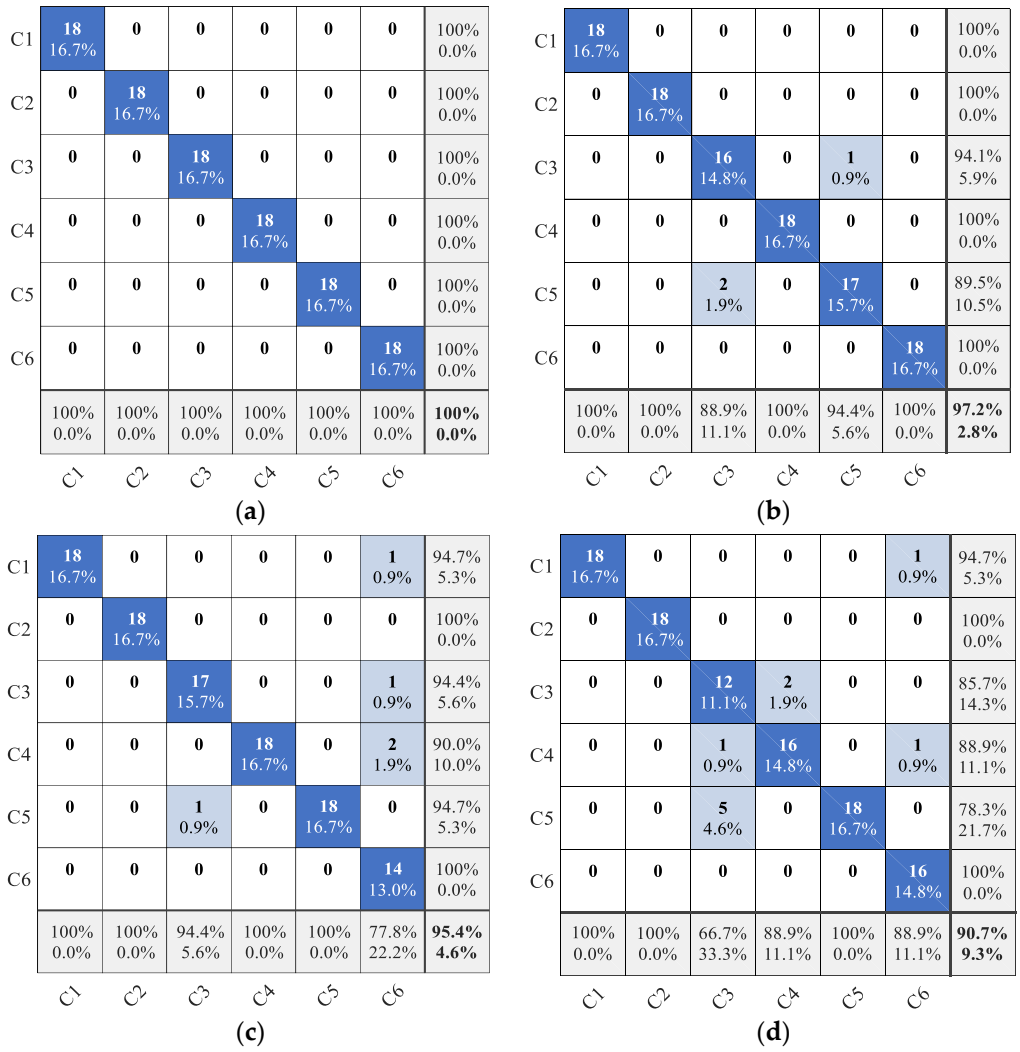

Figure 8. (**a**) VMD + MSE + CNN timber damage identification results; (**b**) ALIF + MSE + CNN timber damage identification results; (**c**) EEMD + MSE + CNN timber damage identification results; (**d**) EMD + MSE + CNN timber damage identification results. In all confusion matrices, the abscissa and ordinate of confusion matrix denote the true label and predicted label of timber damage conditions, respectively.

Table 3. Comparison of classification accuracy of four methods.

Different Methods	Accuracy
VMD + MSE + CNN	100%
ALIF + MSE + CNN	97.2%
EEMD + MSE + CNN	95.4%
EMD + MSE + CNN	90.7%

6. Conclusions and Discussion

This paper proposes a novel timber damage monitoring method using PZT-enabled active sensing and intrinsic multiscale entropy analysis. VMD is used to process the

collected response signals and multiple sets of BLIMFs containing a large number of nonlinear and nonstationary damage characteristics are obtained. Afterwards, MSE values at multiple time scales are calculated and used as condition indicators to measure the complexity of BLIMFs. Finally, feature matrices are constructed and employed as the input of CNN to achieve timber damage monitoring. The main research results of the timber damage monitoring method are as follows:

(1) The sandwich design of the PZT sensor consists of two electrode layers and a layer of PZT material. A wide frequency range of vibration is produced and detected by PZT transducers. Thus, PZT can detect ultrasonic waves to achieve the timber damage monitoring.
(2) VMD and MSE are combined to extract the characteristic information of timber damage. VMD can decompose sine wave signals and can effectively separate the frequency components of signals. MSE can accurately characterize the nonlinear characteristics of timber damage as condition indicators.
(3) CNN has strong feature extraction ability and high generalization capacity, which can accurately extract the features denoting different kinds of timber damage. The utilization of CNN contributes to realization of the identification of timber damage conditions.

In our research, the experimental results validate that the proposed novel approach is promising is the field of timber damage monitoring. In future research, catering to a real and practical scenario, more damage conditions need to be considered, especially with different physical properties such as density and moisture content. Further study will be explored by the authors in the near future.

Author Contributions: This research and development work was carried out in various stages: Conceptualization, methodology, data processing and analysis, writing, editing and review. Conceptualization, methodology, S.G., T.S. and Z.L.; data processing and analysis, L.L., T.S. and Z.L.; writing—original draft preparation, S.G. and H.H.; writing—review and editing, S.G., Z.L. and J.Z. All authors have read and agreed to the published version of the manuscript.

Funding: This research work was supported by National Natural Science Foundation of China under Grant No. 51875416 and 51905388, Natural Science Foundation Innovation Group Program of Hubei Province under Grant No. 2020CFA033, and China Postdoctoral Science Foundation under Grant No. 2020M682492, which are greatly appreciated.

Institutional Review Board Statement: Not applicable.

Informed Consent Statement: Not applicable.

Data Availability Statement: Experimental data will be shared on the first author's ResearchGate, and it is also accessible by email contact with the authors under reasonable requests.

Conflicts of Interest: The authors declare no conflict of interest.

References

1. Ramage, M.H.; Burridge, H.; Busse-Wicher, M.; Fereday, G.; Reynolds, T.; Shah, D.U.; Wu, G.; Yu, L.; Fleming, P.; Densley-Tingley, D.; et al. The wood from the trees: The use of timber in construction. *Renew. Sustain. Energy Rev.* **2017**, *68*, 333–359. [CrossRef]
2. Palma, P.; Steiger, R. Structural health monitoring of timber structures–Review of available methods and case studies. *Constr. Build. Mater.* **2020**, *248*, 118528. [CrossRef]
3. Fang, D.P.; Iwasaki, S.; Yu, M.H.; Shen, Q.P.; Miyamoto, Y.; Hikosaka, H. Ancient Chinese timber architecture. II: Dynamic characteristics. *J. Struct. Eng.* **2001**, *127*, 1358–1364. [CrossRef]
4. Ceccotti, A. Composite concrete-timber structures. *Prog. Struct. Eng. Mater.* **2002**, *4*, 264–275. [CrossRef]
5. Zhang, J.; Huang, Y.; Zheng, Y. A feasibility study on timber damage detection using piezoceramic-transducer-enabled active sensing. *Sensors* **2018**, *18*, 1563. [CrossRef]
6. Wang, T.; Zhang, S.; Yuan, R.; Tan, B.; Lu, M. Lead Zirconate Titanate-based bolt looseness monitoring using multiscale singular spectrum entropy analysis and genetic algorithm-based support vector machine. *Proc. Inst. Mech. Eng. Part C J. Mech. Eng. Sci.* **2022**, 09544062221092714. [CrossRef]

7. Jeon, Y.B.; Sood, R.; Jeong, J.H.; Kim, S.G. MEMS power generator with transverse mode thin film PZT. *Sens. Actuators A Phys.* **2005**, *122*, 16–22. [CrossRef]
8. Das, I.; Arif, M.T.; Oo, A.M.T.; Subhani, M. An Improved Hilbert–Huang Transform for Vibration-Based Damage Detection of Utility Timber Poles. *Appl. Sci.* **2021**, *11*, 2974. [CrossRef]
9. Zhang, Y.; Yuen, K.V.; Mousavi, M.; Gandomi, A.H. Timber damage identification using dynamic broad network and ultrasonic signals. *Eng. Struct.* **2022**, *263*, 114418. [CrossRef]
10. Cooley, J.W.; Lewis, P.A.; Welch, P.D. The fast Fourier transform and its applications. *IEEE Trans. Educ.* **1969**, *12*, 27–34. [CrossRef]
11. Laddada, S.; Si-Chaib, M.O.; Benkedjouh, T.; Drai, R. Tool wear condition monitoring based on wavelet transform and improved extreme learning machine. *Proc. Inst. Mech. Eng. Part C J. Mech. Eng. Sci.* **2020**, *234*, 1057–1068. [CrossRef]
12. Babouri, M.K.; Ouelaa, N.; Djebala, A. Experimental study of tool life transition and wear monitoring in turning operation using a hybrid method based on wavelet multi-resolution analysis and empirical mode decomposition. *Int. J. Adv. Manuf. Technol.* **2016**, *82*, 2017–2028. [CrossRef]
13. Lv, Y.; Yuan, R.; Song, G. Multivariate empirical mode decomposition and its application to fault diagnosis of rolling bearing. *Mech. Syst. Signal Process.* **2016**, *81*, 219–234. [CrossRef]
14. Peng, Z.K.; Peter, W.T.; Chu, F.L. An improved Hilbert–Huang transform and its application in vibration signal analysis. *J. Sound Vib.* **2005**, *286*, 187–205. [CrossRef]
15. Bazi, R.; Benkedjouh, T.; Habbouche, H.; Rechak, S.; Zerhouni, N. A hybrid CNN-BiLSTM approach-based variational mode decomposition for tool wear monitoring. *Int. J. Adv. Manuf. Technol.* **2022**, *119*, 3803–3817. [CrossRef]
16. Wang, Z. Fast algorithms for the discrete W transform and for the discrete Fourier transform. *IEEE Trans. Acoust. Speech Signal Process.* **1984**, *32*, 803–816. [CrossRef]
17. Bentley, P.M.; McDonnell, J.T.E. Wavelet transforms: An introduction. *Electron. Commun. Eng. J.* **1994**, *6*, 175–186. [CrossRef]
18. Yuan, R.; Lv, Y.; Lu, Z.; Li, S.; Li, H. Robust fault diagnosis of rolling bearing via phase space reconstruction of intrinsic mode functions and neural network under various operating conditions. *Struct. Health Monit.* **2022**, 14759217221091131. [CrossRef]
19. Dragomiretskiy, K.; Zosso, D. Variational mode decomposition. *IEEE Trans. Signal Process.* **2013**, *62*, 531–544. [CrossRef]
20. Yuan, J.; Liu, L.; Yang, Z.; Zhang, Y. Tool wear condition monitoring by combining variational mode decomposition and ensemble learning. *Sensors* **2020**, *20*, 6113. [CrossRef]
21. Lv, Y.; Yang, D.; Yuan, R.; Yang, K.; Zhong, H. A novel multivariate signal processing-based fault diagnosis approach of rotating machinery under various operating conditions. *Meas. Sci. Technol.* **2022**, *33*, 075106. [CrossRef]
22. Yang, D.; Lv, Y.; Yuan, R.; Li, H.; Zhu, W. Robust fault diagnosis of rolling bearings via entropy-weighted nuisance attribute projection and neural network under various operating conditions. *Struct. Health Monit.* **2022**, 14759217221077414. [CrossRef]
23. Pincus, S.M. Approximate entropy as a measure of system complexity. *Proc. Natl. Acad. Sci. USA* **1991**, *88*, 2297–2301. [CrossRef] [PubMed]
24. Liu, X.; Zhang, X.; Luan, Z.; Xu, X. Rolling bearing fault diagnosis based on EEMD sample entropy and PNN. *J. Eng.* **2019**, *2019*, 8696–8700. [CrossRef]
25. Zheng, J.; Dong, Z.; Pan, H.; Ni, Q.; Liu, T.; Zhang, J. Composite multi-scale weighted permutation entropy and extreme learning machine based intelligent fault diagnosis for rolling bearing. *Measurement* **2019**, *143*, 69–80. [CrossRef]
26. Richman, J.S.; Moorman, J.R. Physiological time-series analysis using approximate entropy and sample entropy. *Am. J. Physiol.-Heart Circ. Physiol.* **2000**, *278*, H2039–H2049. [CrossRef]
27. Bandt, C.; Pompe, B. Permutation entropy: A natural complexity measure for time series. *Phys. Rev. Lett.* **2002**, *88*, 174102. [CrossRef]
28. Costa, M.; Goldberger, A.L.; Peng, C.K. Multiscale entropy analysis (MSE). *A Tutor. MSE* **2000**, *unpublished*.
29. Jiao, W.; Li, G.; Jiang, Y.; Baim, R.; Tang, C.; Yan, T.; Ding, X.; Yan, Y. Multi-scale sample entropy-based energy moment features applied to fault classification. *IEEE Access* **2021**, *9*, 8444–8454. [CrossRef]
30. Yuan, R.; Lv, Y.; Kong, Q.; Song, G. Percussion-based bolt looseness monitoring using intrinsic multiscale entropy analysis and BP neural network. *Smart Mater. Struct.* **2019**, *28*, 125001. [CrossRef]
31. Lv, Y.; Yuan, R.; Wang, T.; Li, H.; Song, G. Health degradation monitoring and early fault diagnosis of a rolling bearing based on CEEMDAN and improved MMSE. *Materials* **2018**, *11*, 1009. [CrossRef] [PubMed]
32. Yuan, R.; Lv, Y.; Li, H.; Song, G. Robust fault diagnosis of rolling bearings using multivariate intrinsic multiscale entropy analysis and neural network under varying operating conditions. *IEEE Access* **2019**, *7*, 130804–130819. [CrossRef]
33. Yang, D.; Lv, Y.; Yuan, R.; Yang, K.; Zhong, H. A novel vibro-acoustic fault diagnosis method of rolling bearings via entropy-weighted nuisance attribute projection and orthogonal locality preserving projections under various operating conditions. *Appl. Acoust.* **2022**, *196*, 108889. [CrossRef]
34. Liu, H.; Liu, Z.; Jia, W.; Zhang, D.; Wang, Q.; Tan, J. Tool wear estimation using a CNN-transformer model with semi-supervised learning. *Meas. Sci. Technol.* **2021**, *32*, 125010. [CrossRef]
35. Yuan, R.; Lv, Y.; Wang, T.; Li, S.; Li, H. Looseness monitoring of multiple M1 bolt joints using multivariate intrinsic multiscale entropy analysis and Lorentz signal-enhanced piezoelectric active sensing. *Struct. Health Monit.* **2022**, 14759217221088492. [CrossRef]
36. Zhang, Y.; Zhao, Y.; Kong, C.; Chen, B. A new prediction method based on VMD-PRBF-ARMA-E model considering wind speed characteristic. *Energy Convers. Manag.* **2020**, *203*, 112254. [CrossRef]

37. Li, Z.; Lv, Y.; Yuan, R.; Zhang, Q. An intelligent fault diagnosis method of rolling bearings via variational mode decomposition and common spatial pattern-based feature extraction. *IEEE Sens. J.* **2022**, *22*, 15169–15177. [CrossRef]
38. Naranjo-Torres, J.; Mora, M.; Hernández-García, R.; Barrientos, R.J.; Fredes, C.; Valenzuela, A. A review of convolutional neural network applied to fruit image processing. *Appl. Sci.* **2020**, *10*, 3443. [CrossRef]
39. Zhong, H.; Lv, Y.; Yuan, R.; Yang, D. Bearing fault diagnosis using transfer learning and self-attention ensemble lightweight convolutional neural network. *Neurocomputing* **2022**, *501*, 765–777. [CrossRef]
40. Hou, Y.; Zhou, L.; Jia, S.; Lun, X. A novel approach of decoding EEG four-class motor imagery tasks via scout ESI and CNN. *J. Neural Eng.* **2020**, *17*, 016048. [CrossRef]
41. Chen, Y.; Xie, H.; Shin, H. Multi-layer fusion techniques using a CNN for multispectral pedestrian detection. *IET Comput. Vis.* **2018**, *12*, 1179–1187. [CrossRef]
42. Acharya, U.R.; Oh, S.L.; Hagiwara, Y.; Tan, J.H.; Adam, M.; Gertych, A.; San Tan, R. A deep convolutional neural network model to classify heartbeats. *Comput. Biol. Med.* **2017**, *89*, 389–396. [CrossRef] [PubMed]
43. Kuo, C.C.J. Understanding convolutional neural networks with a mathematical model. *J. Vis. Commun. Image Represent.* **2016**, *41*, 406–413. [CrossRef]
44. Narayanan, A.; Kocherla, A.; Subramaniam, K.V. Embedded PZT sensor for monitoring mechanical impedance of hydrating cementitious materials. *J. Nondestruct. Eval.* **2017**, *36*, 64. [CrossRef]
45. Krizhevsky, A.; Sutskever, I.; Hinton, G. ImageNet Classification with Deep Convolutional Neural Networks. *Commun. ACM* **2017**, *60*, 84–90. [CrossRef]